PCCP

Dynamic Article Links ▶

www.rsc.org/pccp

PERSPECTIVE

The complexity of mesoporous silica nanomaterials unravelled by single molecule microscopy†

Timo Lebold, Jens Michaelis* and Christoph Bräuchle*

Mesoporous silica nanomaterials are a novel class of materials that offer a highly complex porous network with nanometre-sized channels into which a wide amount of differently sized guests can be incorporated. This makes them an ideal host for various applications for example in catalysis, chromatography and nanomedicine. For these applications, analyzing the host properties and understanding the complicated host–guest interactions is of pivotal importance. In this perspective we review some of our recent work that demonstrates that single molecule microscopy techniques can be utilized to characterize the porous silica host with unprecedented detail. Furthermore, the single molecule studies reveal sample heterogeneities and are a highly efficient tool to gain direct mechanistic insights into the host–guest interactions. Single molecule microscopy thus contributes to a thorough understanding of these nanomaterials enabling the development of novel tailor-made materials and hence optimizing their applicability significantly.

Introduction

Periodic mesoporous silica materials formed through the cooperative self assembly of surfactants and silica framework

Department of Chemistry and Center for Nanoscience (CeNS), Ludwig-Maximilians-University Munich, Butenandtstraße 11, 81377 Munich, Germany.
E-mail: Christoph.Braeuchle@cup.uni-muenchen.de, Jens.Michaelis@cup.uni-muenchen.de

† This article was submitted as part of a Themed Issue on Single-Molecule Optical Studies of Soft and Complex Matter. Other papers on this topic can be found in issue 5 of vol. 13 (2011). This issue can be found from the *PCCP* homepage [http://www.rsc.org/pccp]

building blocks date back to 1992. At that time scientists of the Mobil company discovered a new class of silica/aluminosilicate hybrid materials, which they called M41S materials.[1,2] In 1998 the portfolio of mesoporous silica materials was enriched by the so-called Santa Barbara Amorphous (SBA) type materials.[3,4] The M41S and SBA type nanomaterials possess a channel network that offers pore sizes ranging from 2–30 nm. Consequently, the porous network is accessible for a wide amount of differently sized and charged guest molecules (dyes, reactants, biomolecules) and these novel materials overcome the long standing pore size constraint of microporous zeolites (pore sizes <2 nm).[5]


Timo Lebold

Timo Lebold is a Postdoc in the Department of Chemistry at the Ludwig-Maximilians-University (LMU) Munich. He studied Chemistry at the Philipps University Marburg and spent 6 months at the University of Cambridge (UK) before he received his PhD at the LMU Munich in 2010. His research interests focus on mesoporous silica nanomaterials and their application in drug-delivery and material science, investigated by single molecule microscopy techniques. During his PhD he was supported by the Elite Network of Bavaria as a member of the International Graduate School NanoBioTechnology.

Jens Michaelis

Jens Michaelis is a Professor for Biophysical Chemistry at the LMU Munich. After receiving his PhD in Physics in 2000, he spent several years as a Postdoc at the University of California, Berkeley, focusing on single-molecule studies of molecular motors. His research interests include the molecular mechanisms that underlie the biological activity of proteins, the mechanical properties of polymer molecules as well as the development of single-molecule methods and super-resolution microscopy. In 2007 he was awarded the Römer Prize of the LMU Munich for young group leaders, in 2009 he received an ERC starting grant and in 2010 the Nernst-Haber-Bodenstein award.

This journal is © the Owner Societies 2011

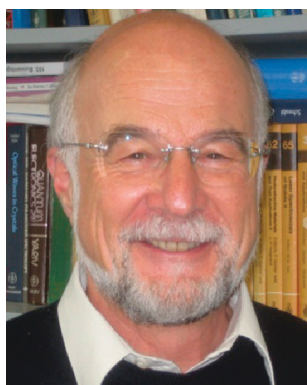*Phys. Chem. Chem. Phys.*, 2011, **13**, 5017–5033 | 5017
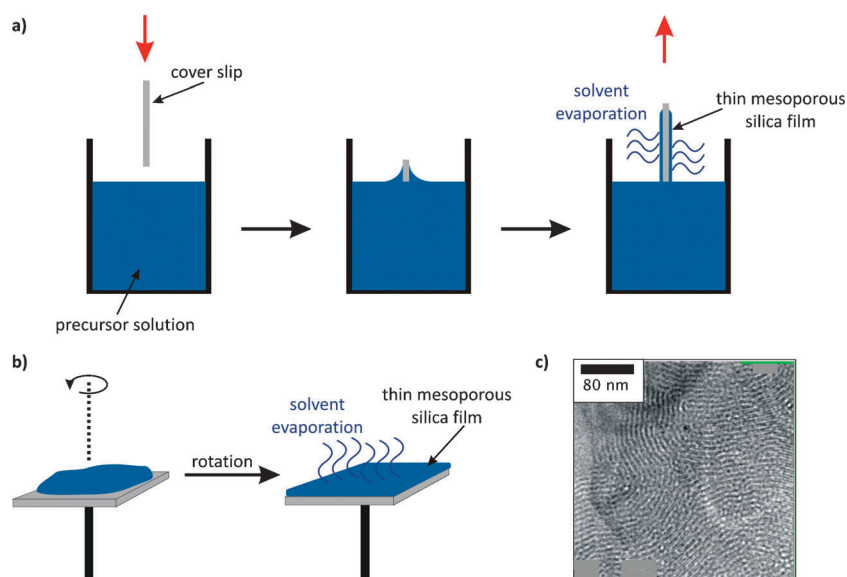
Fig. 1 **Synthesis methods for thin mesoporous silica films.** (a) Dip-coating. The cover-slip is immersed into the precursor solution. Through slow retraction of the cover-slip from the precursor solution a thin film is formed on both sides of the substrate. Solvent evaporation induces the formation of a mesoporous silica structure. The film thickness can be controlled by the cover-slip retraction velocity. (b) Spin-coating. A droplet of the precursor solution is placed onto a cover-slip. Rotating the cover-slip leads to solvent evaporation and the formation of a mesoporous film, whose thickness is critically dependent on the rotation velocity. (c) A typical transmission electron microscopy (TEM) image of a thin mesoporous silica film with a hexagonal pore topology. The image shows domains of parallel aligned and curved channels as well as unstructured defect regions (left upper corner, below the scale bar).

Mesoporous silica materials represent a highly versatile class of materials, since for example the sample morphology can be modified over a wide range from powders to thin films with thicknesses from ∼50 nm to several micrometres. Whereas, spherically shaped mesoporous silica particles of the SBA-type can for example be synthesized through hydrothermal synthesis,[6] mesoporous silica filaments with an ordered channel structure can be created with the help of Anodic Alumina Membranes (AAM, Ano-disc) as structure guiding matrix.[7,8] Throughout this review, we display studies of

mesoporous silica structures in the form of thin mesoporous silica films (see Fig. 1). Thin films are an interesting morphology to study since they can act as coatings on diverse substrates for applications either in catalysis or in drug-delivery. Further, thin films can be prepared with large domains of pores aligned in parallel, which is a desired feature for many applications. Finally, the thin films can be coated on a transparent substrate, *e.g.* glass, which is essential for single molecule investigations.

Thin films of mesoporus silica can basically be synthesized by two methods: dip-coating (Fig. 1a) or spin-coating (Fig. 1b). Both methods start from a precursor solution containing silica building blocks, such as tetraethyl orthosilicate (TEOS) and surfactant molecules as templates in an acidic ethanol/water solution. During dip-coating (Fig. 1a) a cover-slip gets immersed into the precursor solution and slowly retracted again. This leads to the formation of a thin film of solution on the sub-strate, from which the solvent can slowly evaporate. During spin-coating (Fig. 1b) solvent evaporation is caused by rotation of the cover-slip on which the precursor solution was placed. The evaporation of the solvent during either dip- or spin-coating leads to a process called Evaporation Induced Self-Assembly (EISA), which results in the formation of a condensed mesoporous silica structure. There are two synthesis mechanisms that can explain EISA: a two-step mechanism and a cooperative one-step mechanism.[9,10] Prior to EISA, the surfactant concentration inside the precursor solution is below the critical micelle concentration (CMC). This means that no surfactant micelles are present. Next, solvent evaporation increases the surfactant concentration above the CMC. In the two-step mechanism this leads to the formation of a liquid-crystalline phase around which the silica can condense

Christoph Bräuchle studied Physics and Chemistry at the Technical University Berlin and the University Tübingen. He received his PhD at the LMU Munich and spent then one year as a postdoc at IBM in San José, California, USA. After receiving several calls from different universities he took over a Chair of Physical Chemistry at the LMU Munich. His current research focuses on imaging, spectroscopy and manipulation of single molecules and nanoparticles

Christoph Bräuchle

in bio- and nano-sciences. Besides more than 300 publications in international journals, Prof. Bräuchle has won several honors, including the Philip Morris Research award and the Karl Heinz Beckurts Prize 2002. He is also a member of the Bavarian Academy of Sciences and the Academia Europaea.

subsequently. In contrast, the one-step mechanism postulates a cooperative self-organization of the silica precursor and the surfactant below the CMC. In this case, the inorganic silica induces the formation of an ordered hexagonal array of surfactant molecules.

Fig. 1c shows a typical transmission electron microscopy image (TEM) of a hexagonally ordered thin mesoporous silica film. One can clearly see different so-called domains of parallel aligned and curved channels. In the left upper corner of the image unstructured defect regions are visible. Further transmission electron microscopy images of hexagonal

mesoporous silica materials are discussed in the next paragraph (see Fig. 2).

Moreover, by modifying the silica to surfactant ratio, different pore topologies (*e.g.* hexagonal, cubic or lamellar) can be synthesized.[11–13] Schematic views of different pore topologies are shown in Fig. 3a (hexagonal: left panel, lamellar: right panel).

The hybrid system created by embedding a guest molecule in a porous host is called host–guest system. In the pore the guest molecule is embedded inside the surfactant micelle and is "solved" in an ethanol/water mixture that remains within the channels after thin film synthesis. This matrix critically influences the dye diffusion, which was shown for example for a terrylene diimide dye as guest molecule by creating ethanol and chloroform atmospheres.[14] The solvent can help to overcome attractive interactions between the guest molecule and the silica wall, that exist for example due to hydrogen bonding at adsorption sites. Additionally, in order to tune the host–guest interaction, the surface properties of the internal (channel walls) and external surfaces of the materials can be fine-tuned over a large range for example by functionalization of the silica with organic functional groups. Three principal methods have been developed for such organic modifications. The first is the so-called post-synthesis grafting method.[15,16] In this approach the pre-synthesized silica framework is modified with alkoxy or chloro organosilanes.[17,18] An alternative approach is based on post-synthetic substitution of the silica in the material with organometallic compounds.[19–22] Finally, organic modification of mesoporous silica can be achieved by copolymerization of an organosilane with a silica precursor in the presence of the surfactant template.[23,24] This process is called co-condensation.

The high degree of versatility in pore size, topology, morphology and surface functionalization makes the materials an ideal platform for various applications since the host matrix can be tailor-made according to the individual requirements. Consequently, within the recent years a growing number of
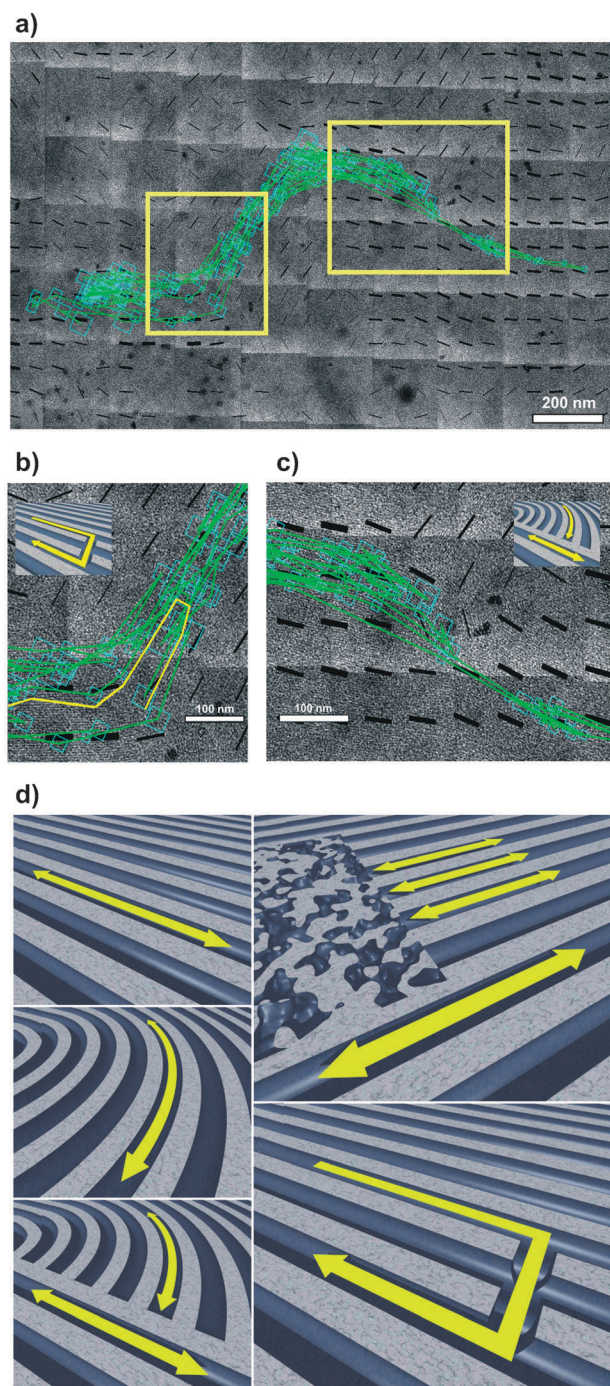
Fig. 2 Correlating dynamic and structural information by combining Single Molecule Microscopy and High-Resolution Transmission Electron Microscopy.[51] Investigation of Brij-56 templated thin silica films. (a) Overlay of an S-shaped trajectory of a single molecule recorded by measuring a series of fluorescence images and determining the center of the single molecule fluorescence for each image with an underlying transmission electron microscopy map. The molecule is exploring regions of parallel aligned channels, with strongly curved areas and domain boundaries indicated by the fast Fourier transform directors (black bars). (b) and (c) Magnified areas of image (a). (b) This part of the trajectory shows a movement perpendicular to the channel direction which occurs through openings (structural defects) in the pore wall between adjacent channels. After changing into a neighbouring channel the molecule reverses its diffusion direction (yellow). (c) A trajectory is displayed in which the molecule repeatedly hits a domain boundary (upper part of the trajectory) before it finds a region where the domains merge and the molecule finds an unobstructed path. The different motional behaviours are schematically depicted in insets in the panels (b) and (c). The light blue boxes in the panels (a)–(c) depict the positioning accuracy. (d) Sketches of structural elements and molecular movements found in these Brij-56 templated hexagonal mesoporous silica thin films.
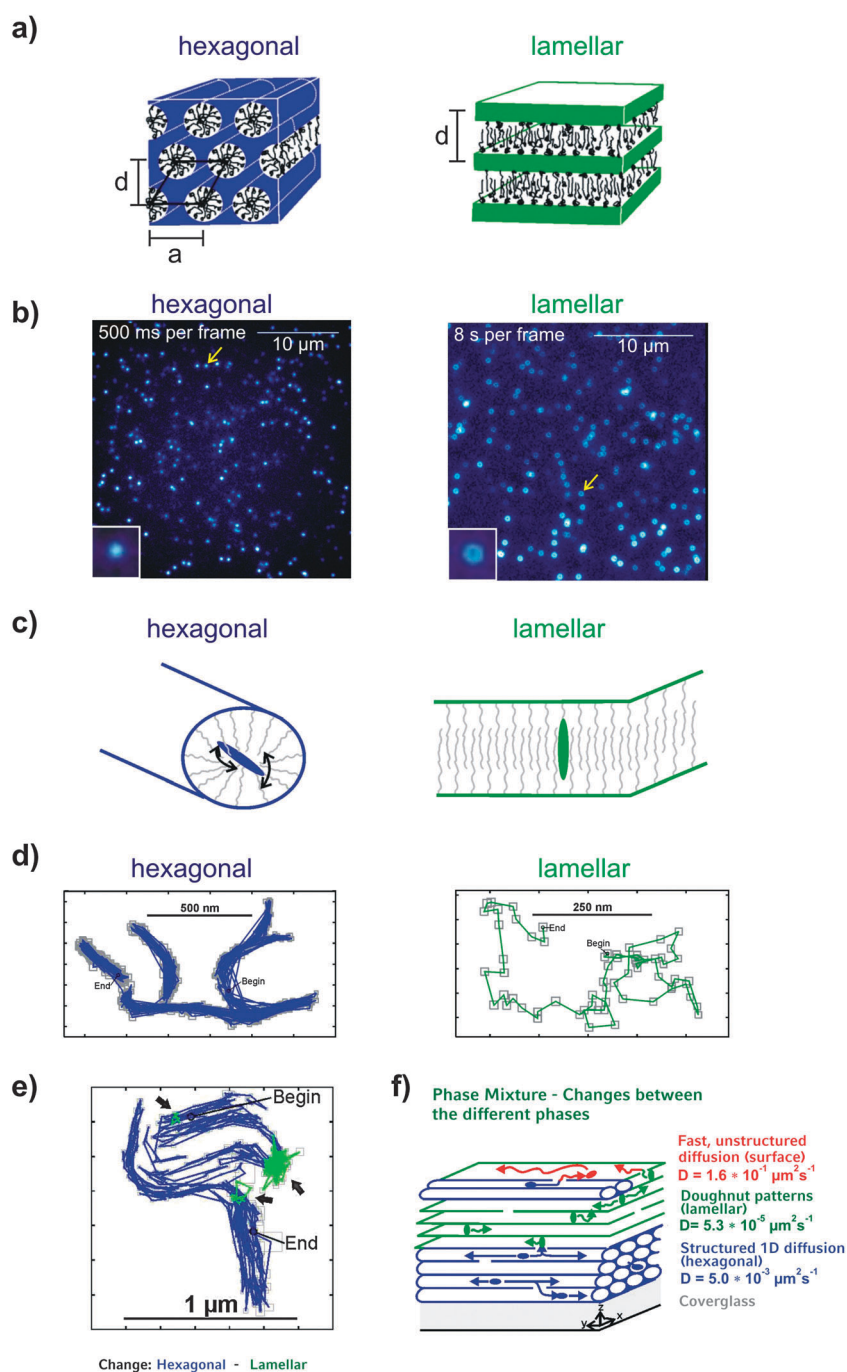
Fig. 3 **Exploration of silica nanostructured channel systems with varying pore topologies using single molecule probes.**[53] (a) Schematic diagrams of Brij-56 templated thin films with hexagonal and lamellar pore topologies. (b) Typical images extracted from wide-field fluorescence movies that show the diffusion of single terrylene diimide derivatives in the thin films. The movies are available as Supporting Information to the publication of Kirstein *et al.*[53] The temporal resolution for the film of the hexagonal phase was 500 ms per frame and for the lamellar phase 8 s per frame. The single molecule image in the hexagonal phase shows only Gaussian-shaped diffraction patterns, whereas in the lamellar phase only doughnut-shaped patterns are observed. The doughnuts are attributed to molecules oriented perpendicular to the substrate. The insets show magnified images of the molecules highlighted by the yellow arrow. (c) Schematic view of the arrangement of the guest molecules inside the hexagonal and lamellar topologies (for detailed measurements of the molecular orientation see Kirstein *et al.*[53]). (d) Sample trajectories from the hexagonal and lamellar phase displaying the typical motional behaviour observed for each phase. The diffusion in the hexagonal phase is nicely structured mapping the channel network, whereas the diffusion in the lamellar phase is random. (e) Trajectory from a molecule diffusing inside a Brij-56 templated thin film with a phase mixture of hexagonal and lamellar phases. The trajectory shows diffusion modes that are characteristic for both phases. The trajectory reveals that the molecule undergoes several changes between the hexagonal (blue parts) and the lamellar phases (green parts, indicated by arrows). (f) Schematic diagram of the diverse diffusion modes observed in the wide-field movies of the phase mixture. Molecules diffusing randomly in the lamellar phase are oriented perpendicular to the surface (doughnuts in the wide-field movies). Structured diffusion over long distances takes place in the hexagonal phase. Molecules on the surface show fast, unstructured diffusion. Transitions between the different diffusion modes are explained by connections between the pore topologies.

applications for this novel class of materials has been suggested, such as molecular sieves,[25] catalysis,[26] chromatography,[27] stabilization of conducting nanoscale wires[28–30] and novel drug-delivery systems[31–35] to mention only some of them.

In order to characterize the intricate host–guest interplay and to maximize the application potential of the porous silica nanomaterials, efficient techniques to investigate the structures are necessary. Standard methods for the investigation and manipulation of nanometre-sized matter such as Scanning Tunneling Microscopy (STM)[36,37] and Atomic Force Microscopy (AFM)[38] can only yield information about the material surface. However, the important processes that govern the host–guest interaction and guest dynamics occur mostly inside the materials. Dynamic information about the diffusion of a guest inside the porous host can be gathered for example with pulsed field gradient NMR,[39] or neutron scattering.[40] However, only non-invasive optical microscopy techniques for observing single molecules, pioneered by Moerner[41,42] and Orrit,[43] yield direct information, firstly about static and dynamic heterogeneities of the host structure, secondly about the behavior of the guests and thirdly about mechanistic details of the host–guest interactions. Furthermore, single molecule microscopy can reveal subpopulations of differently behaving molecules. Single molecule approaches, reviewed for example by Moerner et al.[44,45] or Bräuchle et al.,[46] therefore prevail over classical ensemble techniques since the latter suffer from the inevitable averaging of the observed parameters due to the ensemble population.

In this review, we will show how single molecule microscopy can contribute towards a thorough understanding of mesoporous silica nanostructures and their intricate host–guest interplay by reviewing recent work in that field including an outlook on potential developments. First, we describe a study (Fig. 2) that demonstrates that single molecule data contain a vast amount of information about the structural characteristics of the investigated mesoporous silica host. It is an essential prerequisite for all further studies to prove that individual molecules can act as efficient probes that explore the silica material. In a second study (Fig. 3), we focus on the versatility of the materials by investigating two typical pore topologies for porous silica: hexagonal and lamellar porous systems. The third study (Fig. 4) then draws attention to the structurally and spatially heterogeneous character of these complex materials. Next, the experiments described in Fig. 5 allow the authors to locate the diffusing molecule inside the porous host with an accuracy of one individual channel (5–6 nm). Observing highly dynamic processes with a positioning accuracy in the nanometre range still represents a great challenge to other methods and once more demonstrates the high potential of single molecule experiments for the investigation of these materials. Moreover, spectral and orientational dynamics of dye molecules reveal the complexity of the materials. The last two studies (Fig. 6 and 7) then focus on potential applications of mesoporous silica. For applications in drug-delivery, the drug dynamics inside the carrier system and the drug-release profile should be adjustable in order to realize a so-called depot-effect. Fig. 6 demonstrates how the diffusion dynamics of an incorporated guest molecule can be fine-tuned through organic functionalizations of the porous

silica materials. At the end of the review (Fig. 7), we display a study that demonstrates the applicability of mesoporous silica materials for the delivery of the widely used anti-cancer drug Doxorubicin to tumor cells.

For the sake of clarity, we list in Table 1 key experimental parameters such that the different studies can be compared better. The Table also demonstrates the versatility of the materials.

Correlating dynamic and structural information by combining single molecule microscopy (SMM) and high-resolution transmission electron microscopy (HRTEM)

With this first study, we want to demonstrate that single molecule trajectories are a powerful tool to evaluate the structure of the host matrix since they encode a high amount of information about the host.

Optical microscopy can yield very detailed trajectories of the movement of fluorophores inside mesoporous silica. With that, the porous network and the interconnectivity of the channels can be analyzed in great detail. However, optical microscopy cannot directly image the mesoporous structure of the host system. On the other hand, high-resolution transmission electron microscopy (HRTEM) images offer a distinct means of directly visualizing the channel structure of a mesoporous host and therefore serve as an excellent map of the porous network.[50] By overlaying single molecule trajectories with HRTEM images, the molecular motion inside the structure can be correlated to structural features (dead ends, defects, etc.) of the host. Moreover, gaining information about the behavior of the embedded guest molecules as a function of the local host structure is important for many applications.

For the implementation of this approach, key sample requirements include extremely thin optical-transparent mesoporous films on electron-transparent substrates. For that purpose, thin films templated with the non-ionic surfactant Brij-56 (polyethylene glycol hexadecyl ether) were synthesized with a hexagonal pore order. Through the formation of micelles the surfactant Brij-56 acts as structure guiding agent and determines the topology of the porous network as well as the pore size. By ellipsometry, the films were measured to be 100 nm thick.[51] To obtain highly accurate trajectories of the molecular movement strongly fluorescent dye molecules, such as terrylene diimide (AS-TDI),[47,48] were used for single molecule tracking. In order to guarantee an accurate overlay it is essential to use markers that are visible in both HRTEM and optical microscopy. Good candidates are polystyrene beads with a diameter of 280 nm, since they yield a low fluorescent background, do not interfere significantly with the EISA synthesis and can be accurately localized with both techniques. The markers were added to the synthesis solution of the mesoporous film together with the TDI dye and were incorporated into the pores during evaporation-induced self-assembly of the thin films.[52]

By first recording the trajectories with the optical wide-field microscope, then measuring HRTEM images of the same sample region and finally correlating the beadpositions, a correct overlay of both images can be achieved. This tedious
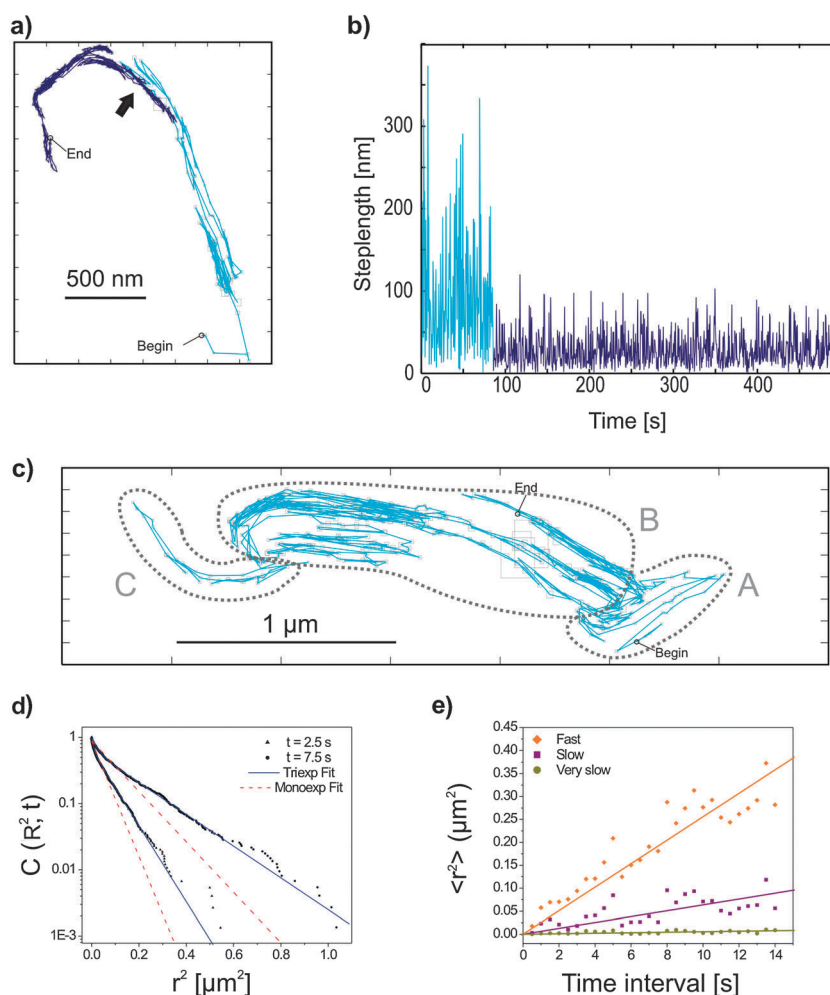
Fig. 4 Analyzing structural and spatial heterogeneities of a Brij-56 templated mesoporous silica films with a hexagonal pore topology.[53] (a) Trajectory of a molecule, that first diffuses fast (light blue) until it becomes instantaneously much brighter and also five times slower (dark blue) after 85 s (see arrow). (b) Plot of the absolute values of the step length against time for the trajectory shown in (a) clearly showing the change in the diffusion behaviour. (c) Trajectory of a molecule diffusing in a structured manner in different domains (A, B, C) of the porous network. (d) Plot of the inverse of the cumulative probability distribution $C(R^2, t)$ for two sample time intervals (t = 2.5 s and 7.5 s). Mono-exponential fits (red dashed line) and tri exponential fits (blue line) are given. (e) Plot of the mean square displacement $\langle r^2 \rangle$ against the time intervals. Fits according to $\langle r^2 \rangle = 2Dt$ for the three different characteristic $\langle r^2 \rangle$ distributions.

procedure provides an overlay accuracy of typically 4 nm to 30 nm, depending on the number of beads in the images.[51] Fig. 2a shows the overlay of a single molecule trajectory with a HRTEM map ($\times 40\,000$ magnification). The map is obtained from many individual HRTEM images. Within each HRTEM image, a fast Fourier transformation (FFT) can be used to determine a FFT director that depicts the average orientation of the pores. Its line thickness provides a measure of the degree of structural order in that region. These directors serve as a good guide for the eye with respect to the orientation of the channels and also provide an overview of the sizes of the domains of parallel aligned pores. Additionally, Fig. 2a shows a single molecule trajectory of a dye molecule moving in that region of the mesoporous thin film. The molecule faithfully follows the pores and maps out specific elements of the host structure.

In Fig. 2b and c, specific regions of Fig. 2a are enlarged to show both the channel structure and the trajectories in greater

detail. In all the three figures, the light blue boxes in the trajectory indicate the positioning accuracy of the determined molecular positions. As these are in the range of 15–30 nm, the molecules' positions cannot be assigned to a single channel, but rather to an ensemble of about three to six parallel channels. Moreover, the diffusion is sampled with an integration time of 200 ms per frame of the recorded movies. Hence, the connecting lines between the trajectory points do not necessarily represent the molecules' actual path but simply provide a method of visualizing the trajectories.

Fig. 2b displays a magnified part of the trajectory (left yellow box in Fig. 2a). Especially interesting is the segment of the trajectory in Fig. 2b, which is highlighted in yellow. One can clearly see that the molecule first moves in one direction along the general backbone of the trajectory (see the FFT directors) before it changes to an adjacent pore and reverses. This lateral motion of the single molecule between neighbouring channels proves the existence of openings in the channel walls that are

invisible in the HRTEM. The inset in Fig. 2b schematically visualizes this motional behavior. Since there are always defects

present in these materials as we will see later, the openings provide the opportunity for the molecule to circumvent
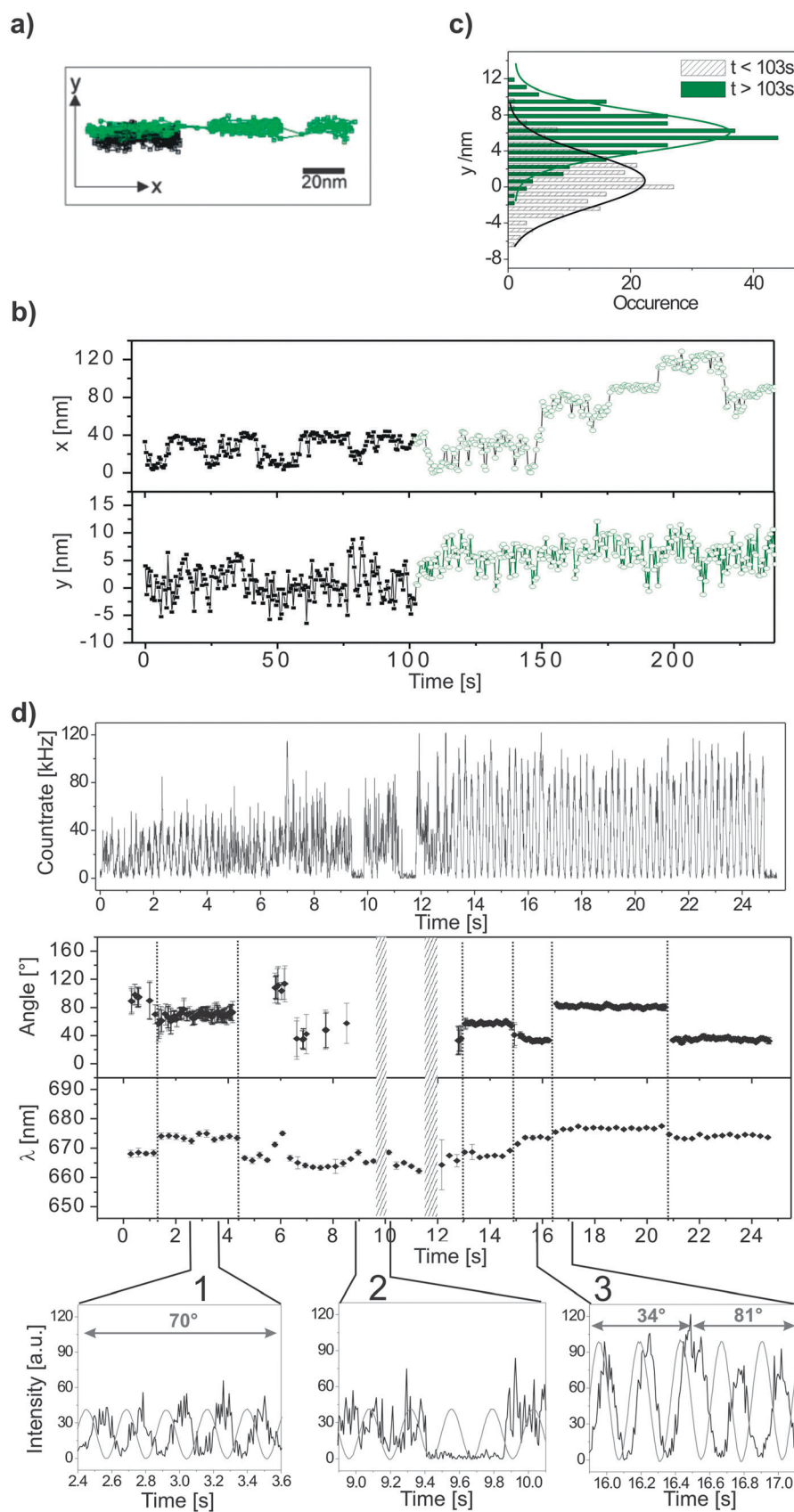
obstructed pores and their existence is thus an advantage for applications such as chromatography or electrophoresis.

The magnification in Fig. 2c highlights another important feature of mesoporous silica structures: a so-called domain boundary. The upper part of the trajectory clearly shows that the molecule bounces back from the domain boundary, *i.e.* a region where the general orientation of the channels changes according to the FFT directors. The schematic inset visualizes this boundary. The channels of the different domains are usually not connected at such a boundary and the molecule thus diffuses into a dead end and needs to turn around. Since the two domains converge, in the lower part of the trajectory the molecule finds an unobstructed way along the channels.

Many more structural elements can be found and correlated with the dynamic behavior of the single molecules as illustrated schematically in Fig. 2d.

These experiments demonstrate that a combination of HRTEM and single molecule optical techniques provides the first direct proof that the molecular diffusion pathway through the pore system correlates with the pore orientation of the hexagonal structure. In addition, the influence of specific structural features of the host on the diffusion behavior of the guest molecules can be clearly seen. Furthermore, single molecule microscopy contributes valuable information about pore connectivities and accessibilities that are invisible by HRTEM. With this approach, it is possible to determine, in unprecedented detail, how a single fluorophore travels through linear or strongly curved sections of the hexagonal system, why it changes its apparent diffusion constant and how it bounces off dead ends due to domain boundaries. Additionally, this technique helps to detect less-ordered defect regions that minimize the functionality and applicability of the material. Also leaky channels within the otherwise well-ordered periodic structure that allow a molecule to penetrate into adjacent channels and may affect the functionality of the material can be identified. Finally, such correlative studies highlight the structural heterogeneity of these mesoporous materials.[51]

Exploration of silica nanostructured channel systems with varying pore topologies using single molecule probes

As mentioned above, one key advantage of mesoporous silica structures is their high degree of versatility which makes them an attractive platform for various applications. In this section, variations in the pore topology of Brij-56 templated mesoporous films and their implications on the behavior of incorporated

guest molecules will be investigated. Modification of the mesoporous topology can be done by changing the molar ratio between the surfactant and the silica oligomers in the EISA precursor solution. Since the previous section demonstrated that single molecule microscopy is an efficient tool for investigating the silica host structure and visualizing the host–guest interactions, we will focus again on single molecule fluorescence experiments in combination with tracking of individual dye molecules in the thin films.

To discuss the general principles we will concentrate on three different sample types. Two of these consist of a single, pure mesophase: hexagonal and lamellar (Fig. 3a), which can be synthesized with a low or a high surfactant/silica molar ratio, respectively. Additionally, also samples with a phase mixture can be synthesized by choosing an intermediate ratio. For the lamellar phase the mean pore-to-pore distance d (see Fig. 3) is typically 6.1 (± 0.1) nm and for the hexagonal phase it is 6.3 (± 0.1) nm according to X-ray diffractometry patterns.[53] These are just average values. The recorded peaks show a distinct broadness, which indicates that a distribution of pore-to-pore distances and thus pore sizes is present in the samples. The wall thickness in these systems are about 1–2 nm, hence a pore diameter of 4–5 nm is filled with template and provides the space for molecular movement.

Fig. 3b shows typical images extracted from movies obtained on a widefield fluorescence microscope. Thin mesoporous films with a purely hexagonal phase (left side) and a purely lamellar phase (right side) are shown. In the widefield image of the hexagonal phase only Gaussian-shaped diffraction patterns are observed (see inset, left side), whereas the single molecules in the lamellar phase appear as doughnuts (see inset, right side). Such doughnut-shaped diffraction patterns have previously been assigned to single molecules with their translation dipoles (here, the long molecular axis of TDI) aligned along the optical axis of the microscope.[54] One should note that the observation of two clearly distinct populations (purely Gaussian- and purely doughnut-shaped) represents a special case resulting from the structure of the utilized TDI dye.[55] Feil *et al.* investigated in detail how the Gaussian/doughnut ratio depends on the structure of the utilized dye and they showed that a variation in the structure of the dye allows for a much broader spectrum of interactions.[56] In the present case, the doughnut-shaped molecules represent molecules in the lamellar phase that are oriented perpendicular to the layers of the silica and thus to the glass substrate, whereas Gaussian-shaped patterns stem from molecules in the hexagonal phase

---

Fig. 5 Analyzing the translational, spectral and orientational dynamics of a terrylene diimide dye inside CTAB template porous silica films with high accuracy.[14,57] (a) Trajectory of the dye molecule inside macroscopically sized unidimensional domains of the thin films. An animation of this trajectory is shown in Movie 6 of the Supporting Information of the study of Jung *et al.*[14] (b) Projected x and y coordinates for a single TDi molecule diffusing at least in two distinct neighbouring pores. While in the first 103 s the molecule diffuses back and forth in one pore (black squares), it then switches to another pore, where it presumes its lateral diffusion (green circles). (c) Histograms of the y lateral coordinate for the time intervals before (black striped bars) and after (green full bars) the time $t = 103$ s together with their Gaussian fits (bottom). The two maxima are separated by 5–6 nm. (d) Orientational and specral behaviour of TDI in a CTAB templated film. The upper panel shows the polarization-dependent fluorescence trace. The middle and lower panels give the angular and spectral trajectory after data analysis. The insets 1, 2 and 3 represent excerpts from the curve. The continuous thin line in the insets corresponds to the excitation polarization. (1) A stable orientation of $\sim 70°$ over a period of seconds. (2) Segments where no preferred orientation could be assigned and a blinking event occurred. (3) Time window with a distinct orientational jump from 34° to 81°.
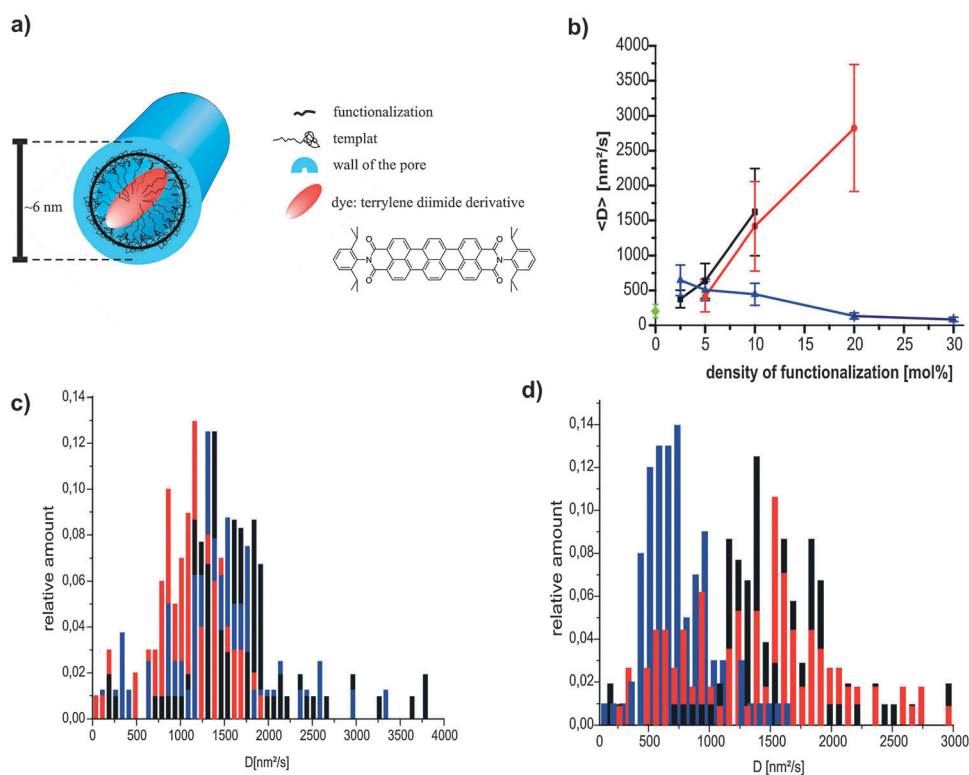
Fig. 6 **Tuning single molecule dynamics in functionalized mesoporous silica.**[66] (a) Sketch of a terrylene diimide dye molecule within one pore of a functionalized mesoporous silica structure. All constituents are drawn to scale. The chemical structure of the dye is displayed on the right. (b) Correlation of the mean diffusion coefficients $\langle D \rangle$ with the functionalization densities, including data for the unfunctionalized film, given at zero density (black: propyl, red: cyanopropyl, blue: phenyl, green: unfunctionalized). The bars indicate the width of the distribution of the D-values due to the heterogeneity of the samples, and not to any error in their determination. (c)–(d) Influence of the (c) alkyl chain length (red: methyl, blue, ethyl, black: propyl) and (d) the polarity of the functional groups (red: cyanopropyl, blue: trifluoropropyl, black: propyl) on the diffusion dynamics of the guest molecules. The films in (c) and (d) were synthesized with 10 mol% functionalization density and measured at 30% relative humidity.

(see Fig. 3c for a schematic) that can rotate freely. The utilized TDI dye possesses an alkyl group at one end of the fluorophore.[53] This alkyl group might favour a parallel orientation of the dye to the template alkyl groups. This could explain why a free rotation of the dye inside the lamellas is hindered. It is important to note that the exposure times for the movies in the two different phases differ by a factor of 16, as the molecules in the hexagonal phase diffuse much faster than in the lamellar phase. The above suggested interaction of the alkyl group of the dye and the template would also contribute to a deceleration of the dye. Typical single molecule trajectories for the different phases are depicted in Fig. 3d. Molecules in the hexagonal phase travel generally in a highly non-random manner over distances of several micrometres during the acquisition time of the movie (500 s). In contrast, the doughnut-shaped patterns in the lamellar phase show random diffusion on a much slower timescale and cover areas smaller than 1 μm during the same time interval of 500 s.
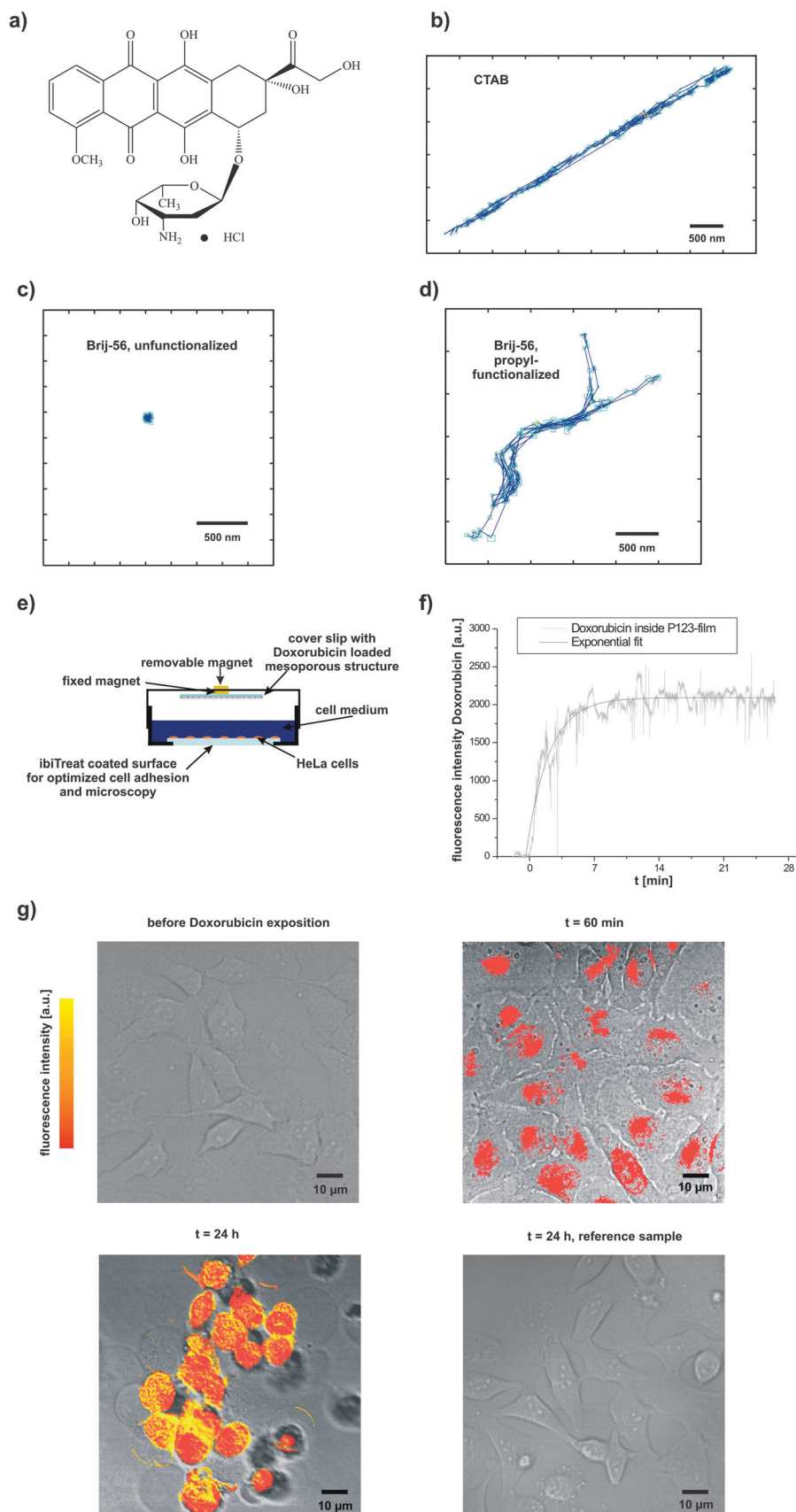
It is extremely interesting to also investigate the diffusion of dye molecules in samples showing a phase mixture of hexagonal and lamellar mesophases. Due to the mixture of phases, Gaussian-shaped and doughnut-shaped patterns can be found in the same region of the thin film. Yet, on the basis of their diffraction pattern and diffusive behavior two further populations of molecules can be detected. This very small third

population consists of molecules that diffuse much faster, without showing any particular structure in their trajectories. These molecules can be removed by washing the surface of the thin films with water, which clearly indicates that the molecules were on the surface of the film. Finally, a fourth population of molecules can be found whose mode of motion changes repeatedly between the previously described populations. A specific example is shown in Fig. 3e. Again, as in the pure hexagonal phase the shape of the trajectory explored by the Gaussian pattern clearly reflects the underlying pore structure of the hexagonal phase. The molecule in Fig. 3e changes three times from a Gaussian spot to a doughnut and back (see black arrows), with different residence time in each phase. Such switching phenomena clearly show that the two phases are actually connected, most likely *via* structural defects at the phase boundaries. Interestingly, other cases were also observed where the molecule switched several times from a Gaussian to a doughnut-shaped pattern at exactly the same position. This showed that, on occasion, the molecules pass repeatedly in a lateral direction through the same defect region between phases.

A general schematic diagram of the different phases present in the film and the migration within, as well as between, the phases is shown in Fig. 3f. Thus, the structure of the trajectories, the diffusivities and the orientation of single molecules are

clearly distinctive for molecules travelling in the different mesophases. Through a single molecule optical analysis, the relative proportion of the different phases and their degree of interconnectivity can be directly assessed.

a)

b) CTAB — 500 nm

c) Brij-56, unfunctionalized — 500 nm

d) Brij-56, propyl-functionalized — 500 nm

e) cover slip with Doxorubicin loaded mesoporous structure
removable magnet
fixed magnet
cell medium
ibiTreat coated surface for optimized cell adhesion and microscopy
HeLa cells

f) fluorescence intensity Doxorubicin [a.u.]
Doxorubicin inside P123-film
Exponential fit
t [min]

g) fluorescence intensity [a.u.]
before Doxorubicin exposition — 10 µm
t = 60 min — 10 µm
t = 24 h — 10 µm
t = 24 h, reference sample — 10 µm

Table 1 **Experimental conditions for the discussed studies.** Brij-56: Polyethylene glycol hexadecyl ether, CTAB: Cetyltrimethyl ammonium bromide, Pluronic P123: tri-block copolymer poly(ethylene oxide)$_{20}$-poly(propylene oxide)$_{70}$-poly(ethylene oxide)$_{20}$

	Surfactant	Pore-to-pore distances [nm]	Guest molecules	Topology
Fig. 2	Brij-56	6.5–7.0	AS-TDI[47,48]	hexagonal
Fig. 3 + Fig. 4	Brij-56	6.3 (hexagonal), 6.1 (lamellar layer spacing)	AS-TDI[47,48]	hexagonal lamellar
Fig. 5	CTAB	4.2	AS-TDI[47,48]	hexagonal
Fig. 6	Brij-56	5.5–6.2 (due to different organic functionalizations)	DIP-TDI[49]	hexagonal
Fig. 7	CTAB, Brij-56 Pluronic P123	4.4 (CTAB), 5.6 (Brij-56, functionalized), 6.1 (Brij-56, unfunctionalized), 10 (P123)	Doxorubicin hydrochloride	hexagonal

Analyzing structural and spatial heterogeneities of mesoporous silica films using single molecule microscopy

Due to the synthesis conditions, the chemical nature of the precursors of the porous silica and the reversibility of the underlying condensation reactions, the materials usually show heterogeneities. The experimental data presented in this section demonstrates the potential of single molecule microscopy and single particle tracking methods to reveal these heterogeneities.

Fig. 4a shows the trajectory of an individual molecule observed in a hexagonal phase of a Brij-56 templated thin silica film. The trajectory reveals a structural heterogeneity of the sample by showing different spatially separated diffusion regimes (light and dark blue). The molecule first diffuses with a diffusion coefficient typical for diffusion in the hexagonal phase ($D = 5.3 \times 10^1$ nm^2 s^{-1}, light blue part of the trajectory) but after 85 s the molecule becomes much brighter and diffuses more slowly, with a five times smaller effective diffusion coefficient (dark blue) for the rest of the time. The arrow indicates the region where the diffusion mode changes. This instantaneous change in diffusivity can be visualized by plotting the step length as an absolute value against time, as shown in Fig. 4b. The different diffusion regimes can clearly be distinguished due to the significant reduction of the step lengths. These distinct regimes may arise from structural heterogeneities of the materials, e.g. from a change in the local environment of the molecule, such as a slight variation in the pore diameter or a local variation of the amount of template. Such a variation in the local environment can indeed drastically influence the spectral properties of the molecule and thus also its fluorescence intensity.[57,58] This is shown in the next paragraph (see Fig. 5), where spectral dynamics are investigated in more detail.

However, even if the molecules do not show spatially separated diffusion regimes, the observed diffusional behaviour is often not homogeneous. This is shown by the following analysis. The molecular trajectory of Fig. 4c shows a molecule that explores at least three different domains, indicated as A, B and C. The channels in A are oriented perpendicular to the channels in B and a kink separates domains B and C. For this molecule a detailed analysis of the diffusion behavior was done by analyzing the distribution of squared displacements r^2. This distribution can be visualized in two ways: either in the form of a histogram or through cumulative probabilities.[59,60] The analysis of probability distributions (instead of histograms) allows for a more precise analysis and avoids any loss of information due to binning of the histogram. Hence, the following analysis was done by plotting the inverse of the cumulative probability $C(R^2,t)$ of the squared displacements r^2 for different time lags t. The data was fitted with multi-exponential decay functions:

$$C(R^2, t) = \sum_{i=1}^{n} C_i * \exp\left(-\frac{R^2}{\langle r_i^2(t) \rangle + \delta^2}\right) \qquad (1)$$

where c_i is the amplitude of the different exponential components, $\sum_{i=1}^{n} C_i = 1$, $\langle r_i^2(t) \rangle$ are the characteristic values for the mean-square displacement (MSD) and δ^2 corresponds to the positioning accuracy.

Regular diffusion should result in a monoexponential decay ($n = 1$), giving a characteristic value for the MSD $\langle r_i^2(t) \rangle$ for each time lag t. Fig. 4d shows the inverse of the cumulative probability distributions for two sample time intervals ($t = 2.5$ s and 7.5 s). Here, the data cannot be fitted with a monoexponential decay function (red dashed lines in Fig. 4d). Tri-exponential decay functions ($n = 3$) were found to describe the data best (blue solid lines), giving three characteristic $\langle r_i^2(t) \rangle$ values for each time lag. These values are plotted

◀

Fig. 7 **Drug-delivery of the anti-cancer drug Doxorubicin with mesoporous silica nanomaterials.**[70] (a) Structure of the cytostatic drug Doxorubicin hydrochloride. (b)–(d) Exemplary trajectory of a single Doxorubicin molecule inside a (b) CTAB, (c) unfunctionalized Brij-56 and (d) propyl-functionalized Brij-56-templated film. The small blue squares indicate the positioning accuracy for each point in the trajectory, which depends on the signal-to-noise ratio (∼35 nm for CTAB and ∼40 nm for Brij-56-templated samples). While in panels (b) and (d) the molecules are mobile, (c) depicts an immobile molecule appearing as a spot. (e) Sample setup. The sample consists of a μ-Dish filled with cell medium and HeLa cells adhered to the bottom of the dish. On the upper side of the dish, a coverslip with a Doxorubicin-loaded mesoporous structure is held using magnets. Upon removing the magnet, the sample is immersed into the cell medium, which can flush the pores of the delivery system and trigger the drug release. (f) Release kinetics of Doxorubicin from a Pluronic P123-templated thin film. The release was monitored via the rise of fluorescence intensity of Doxorubicin 50 μm above the bottom of the μ-Dish during time (grey curve). The black line shows an exponential fit to the data, according to eqn (3). (g) Live-cell measurements. Overlay of confocal transmission images (grey) and Doxorubicin fluorescence (red). Images before (upper left panel), 60 min (upper right panel) and 24 h (lower left panel) after adding the Doxorubicin-loaded delivery system are shown. As reference an image is shown that was recorder 24 h after adding an unloaded drug-free delivery system (lower right panel).

against time in Fig. 4e. Each of the different sets of $\langle r_i^2(t)\rangle$ values was fitted with the Einstein-Smoluchowski equation for random diffusion in one dimension:

$$\langle r_i^2(t)\rangle = 2Dt \qquad (2)$$

giving values of $D_1 = 1.3 \times 10^4$ nm^2 s^{-1}, $D_2 = 3.2 \times 10^3$ nm^2 s^{-1} and $D_3 = 2.8 \times 10^2$ nm^2 s^{-1}. These large differences imply that the molecule is diffusing in at least three types of environments. However, it can be shown that the three diffusion regimes are not spatially separated. The step sizes corresponding to these three diffusion modes are equally distributed over all parts of the track in contrast to Fig. 4b. They are not segregated in one or other of the domains A, B or C. The mobility of the molecule does not differ significantly from one domain to the other. Instead, owing to structural heterogeneities, the environment within one channel system changes strongly along the pathway of the molecule. These heterogeneities are revealed by the molecule continuously changing its mode of motion between at least three diffusion coefficients. Therefore, its diffusion cannot be described as a simple Brownian motion. An interpretation of these results could actually be a range of diffusion coefficients due to variations of the local environment of the molecular probe.

Hence, this example of trajectory analysis demonstrates that the diffusion coefficients vary not only between different phases (as shown in the previous section) or between trajectories of individual molecules within one phase, but can also change within the same trajectory of an individual molecule. These heterogeneities are only revealed through single molecule microscopy and would have been obscured by ensemble methods due to the inevitable averaging associated with these methods.

Analyzing the translational, orientational and spectral diffusion of guest molecules inside mesoporous silica with high accuracy

The single molecule studies presented so far yielded very detailed insights into the nature of the porous silica materials. However, in the previous studies the single molecules could not be localized with an accuracy of a single individual channel. Yet, reaching this high degree of accuracy in the tracking of the fluorophore allows for an accurate description of the path of the single molecule and observation of jumps between neighbouring pores. A good system to realize this aim are cetylhexyltrimethylammoniumbromide (CTAB) templated and hexagonally ordered mesoporous silica films since the diffusion coefficient in this system is much smaller due to the changed pore size. In addition, a higher laser power (0.50 kW cm^{-2} at the entrance of the objective) compared to standard single molecule experiments also contributes to an increase in positioning accuracy.[14] However, this gain in accuracy can only be achieved at the expense of the length of the observed trajectories. Due to the high laser power, the molecules photobleach faster and thus the trajectories are shorter in time. In order to record a statistically relevant amount of information, the data must be acquired using a high frame rate (500 ms per frame). These setup parameters allow the authors to achieve a localization with unprecedented accuracy ($\sigma = 2$–3 nm for the brightest molecule).

Fig. 5a displays the trajectory of a single terrylene diimide derivative diffusing in linear oriented macroscopically sized domains of a CTAB templated thin silica film, measured under a chloroform atmosphere.[14] The trajectory is divided into two parts (green and black). The corresponding $x(t)$ and $y(t)$ graphs obtained from the trajectory are displayed in Fig. 5b. The two distinct parts of the trajectory cover the time intervals before (black) and after (green) 103 s. By inspection of the graph one can already assume that the molecule laterally penetrates into a neighbouring channel at this time. Fig. 5c analyzes the data of the trajectory in even greater detail by displaying the histograms of $y(t)$ before (green full bars) and after (black dashed bars) 103 s. These distributions are clearly distinct and can be fitted by two Gaussian curves with a maximum at 0.6 and 6.1 nm and standard-deviations $\sigma_1 = 2.9$ nm and $\sigma_2 = 2.3$ nm respectively. Thus, this data show a molecule switching between pores separated by 5–6 nm. The $x(t)$ graph in Fig. 5b extracted from the trajectory of Fig. 4a show a back and forth movement of the molecule which remains clearly confined between $x = 0$ and $x = 40$ nm during the first 150 s of the trajectory. After this time, the molecule finds its way out of this confined region and is able to diffuse further.

In summary, the experimental trajectory described above reveal the existence of connectivities between neighbouring channels, that are invisible to other techniques, and shows that guest molecules can utilize these openings to circumvent a blocked channel. A similar lateral mobility was observed in Fig. 2b. However, the high localization accuracy of $\sim$2–3 nm achieved in the study depicted here, allows for the first time to attribute the lateral diffusion to a switching between two neighbouring channels. The motion of the molecule throughout the porous network was thus described with unprecedented detail.

However, not only the translational dynamics of guest molecules inside CTAB templated mesoporous silica can be investigated by single molecule microscopy with great detail, this method also allows us to extract detailed information about the orientational dynamics of the guest molecules inside the porous host. In order to determine the orientation of the guest molecules a confocal laser scanning microscope can be used in combination with a rotating $\lambda/2$ retardation plate, which can be inserted into the optical setup below the objective. With the help of that plate the excitation light gets modulated in polarization. Depending on its orientation, the molecule fluoresces with a distinct modulated intensity trace from which the molecular orientation can be determined.[57]

Fig. 5d shows a single molecule experiment, where the orientational behavior of the guest dye is investigated in great detail. The polarization-dependent intensity trace is shown in the upper panel of the figure. The middle graph shows the extracted angular trajectory $\Phi(t)$. Only those data points are displayed for which a well-defined orientation can be determined, *i.e.* the orientation is constant during at least one period of the polarization modulation. However, sometimes the molecules also undergo rapid reorientation (omitted points in graph), such that stable orientations cannot be determined. Moreover, also blinking events, where the molecule rests in a photophysical dark state, can be observed (hatched segments).

The time scales on which the orientational dynamics occur range from below the temporal resolution of the experiment (300 ms) to tens of seconds. This can be illustrated by some examples: the insets 1, 2 and 3 which are magnified from the complete trace shown in Fig. 4d. Segment 1 shows that orientations may remain stable on a time scale of seconds. This indicates that strong adsorption sites in the material are accessible to the moving molecule. Adsorption of the molecules may result from direct contact with silica walls, electrostatic interactions with the cationic CTAB template as well as interactions at defect sites (see Fig. 2d). The adsorption duration can then be used as a measure for the interaction strength.

In contrast, inset 2 shows a different characteristic behavior. Here, the molecule undergoes rapid orientational dynamics for a period of seconds. This indicates the presence of regions in which the interactions between the molecule and the matrix are weaker. In this region, the molecule is continuously tumbling between different environments.

Moreover, inset 3 shows an abrupt reorientation, in contrast to the more commonly observed phenomenon, where a period of high dynamics is found in between two adsorption events, as described above. In this example, the movement itself is much faster than the resolution limit. The molecule starts with an orientation of $34° ± 2°$ and jumps to $81° ± 2°$. Later in the trajectory (at about 21 s), as can be seen in the middle graph, the molecule switches back abruptly to the same angle of $34°$. This particular case shows a molecule switching abruptly back and forth between preferential orientations. This switching is likely caused by sites where two stable positions, *i.e.* two minima in the effective potential are present. This is a clear example of a situation where additional information about the molecule, for example its emission spectrum, could help to distinguish between two plausible explanations. Spectral dynamics can be measured at the same time as orientational dynamics (see Fig. 5d) with the help of a prism-CCD-spectrometer.[57] This allows for a correlation between spectral and orientational dynamics. For clarity, it is best not to display the entire spectrum but to show only the spectral position of the emission maximum, $\lambda_m(t)$. Several typical features can be observed: Firstly, the presence of periods during which the maximum of the emission spectrum remains at a constant value, thus yielding a plateau in the time trace. Each plateau in the spectral trajectory can be correlated to a plateau in the orientational trajectory, in the same time range. Secondly, spectral and orientational jumps can be seen in the whole time trajectory. These jumps are usually correlated neither in size nor in direction. However, sometimes one can also observe reversible jumps. An example is seen in the three last plateaus that correspond to two distinguishable spectral positions (674, 677 nm) and can be assigned to the two angular positions (34° and 81°), as discussed above. This further strengthens the argument that in these last periods (from 14.8 to 24.5 s) the molecule under investigation is switching back and forth between two well-defined adsorption sites.

To summarize, the individual molecules explore various environments in which the time scale of the orientational dynamics varies dramatically. In one extreme case a molecule may stay at a specific well-defined orientation, at a strong adsorption site for many seconds—indicated by a constant orientation angle. On the other hand, a molecule can be found to undergo fast orientational dynamics that last for a period of several seconds, if it is within a region in which the host–guest interactions are comparatively weak and the molecule is able to sample different areas. The characterization of such adsorption processes is especially interesting for catalytic reaction sites.

Tuning single molecule dynamics in mesoporous silica with the help of organic functionalizations

So far, we have thoroughly investigated the material properties of mesoporous silica host–guest structures. The following sections now summarize studies that highlight potential applications of these novel materials. Mesoporous silica has already been used for numerous applications as mentioned above. For many of these applications, the mesoporous materials are expected to show enhanced properties when their inner channel walls are functionalized with organic moieties. The key idea behind the functionalization is to influence the diffusion dynamics of the incorporated guest molecules by fine-tuning the host–guest interaction. A decelerated diffusion for example is particularly important for drug-delivery systems. An ideal drug carrier should show a so-called depot-effect, which is a retarded release of the drug at a slow rate over a prolonged period of time.[33,61–63] This could maximize the therapeutic effects significantly. Tuning the diffusion dynamics by organic modification of the channels wall might provide means for achieving such an effect.

A prominent method for the organic functionalization of mesoporous silica is the so-called co-condensation method.[64,65] In this case, organic modification of mesoporous silica can be achieved by copolymerization of an organosilane with the silica precursor (tetraethyl orthosilicate) in the presence of the surfactant template. The advantage of this method is that it enables homogeneous incorporation of the organic groups into the walls of the mesoporous films (Fig. 6a). Single molecule microscopy provides an excellent means to study the effects the functionalization excerts on incorporated guest molecules.[66] Different approaches can be used to influence the mobility of the guest molecule. First, the influence of the functionalization density on the diffusion dynamics of the dye can be examined. Fig. 6b shows that the extracted mean diffusion coefficient $\langle D \rangle$ of the dye molecules correlates to the density of functionalization for the differently functionalized samples. Secondly, one can compare different types of functionalizations, such as propyl- (black line), cyanopropyl- (red line) and phenyl-functionalized (blue line) samples. The $\langle D \rangle$-values of the propyl- and cyanopropyl-functionalized samples increase substantially with increasing functionalization density (with a sevenfold and fourfold factor respectively). In contrast to these organic groups with flexible chains, the $\langle D \rangle$-values for phenyl-functionalized samples decreased with increasing functionalization density. Here, the dyes inside the films are slowed down by almost one order of magnitude, from $\langle D \rangle = 650$ nm^2 s^{-1} (2.5 mol%) to $\langle D \rangle = 80$ nm^2 s^{-1} (30 mol%).

A better understanding of these effects can be achieved by studies systematically investigating different functional

This journal is © the Owner Societies 2011

Phys. Chem. Chem. Phys., 2011, **13**, 5017–5033 | 5029

groups.[66] Fig. 6c shows the diffusion data for aliphatic functional groups with different alkyl chain lengths (methyl, ethyl and propyl). The change in diffusion coefficients due to different alkyl groups is less significant than the change due to different functionalization densities discussed before. However, an increase in diffusivity can be observed for increasing alkyl chain lengths; the mean diffusion coefficient increases from 1100 to 1620 nm^2 s^{-1} (from methyl to propyl functionality). Samples with longer aliphatic chains (pentyl and octyl) do not yield reproducible data as the structural organization of these films was insufficient.

Fig. 6d displays the influence of functional-group polarity on the diffusion coefficients by comparing propyl-, cyanopropyl- and trifluoropropyl-functionalized films. The strongly polar trifluoropropyl groups decrease the mean diffusion coefficient of the dye to about one-half (740 nm^2 s^{-1}) of those of propyl- and cyanopropyl-functionalized films (1620 nm^2 s^{-1} and 1420 nm^2 s^{-1}). Thus, increasing the polarity of the functional groups leads to a decrease in dye dynamics in the case of TDI.[66]

The described data show that the incorporation of functional groups has a profound influence on the diffusional behavior of dye molecules inside surfactant-containing mesoporous silica films. The advanced single molecule microscopy techniques are uniquely suited to reveal the mechanistic details of the host–guest interactions. Again, molecular diffusion proved to be heterogeneous both in space and time. The functional groups are an efficient tool to tune the diffusion dynamics of the guest molecules within one order of magnitude. A deceleration of the guest dynamics is a particularly interesting phenomenon, since this can set the basis for the generation of a depot effect, i.e. the retarded release of the drug over a prolonged period of time.

Nanostructured silica materials as drug-delivery systems for the anti-cancer drug Doxorubicin

Surfactant-templated mesoporous silica materials possess an enormous potential as drug-delivery system as will be shown now using the example of the delivery of the anti-cancer drug Doxorubicin hydrochloride (Fig. 7a). Doxorubicin and its analogues are widely used in chemotherapy, for example, for the treatment of Kaposi's sarcoma,[67] ovarian carcinoma[68] or breast cancer.[69] However, Doxorubicin shows also a especially high renal and cardiac toxicity, which limits its therapeutic applications. Novel drug-delivery strategies for that drug are thus urgently needed.

Since the choice of the specific drug carrying system is dependent on the particular application it is important to experimentally compare different host systems such as (i) CTAB-templated films, (ii) Pluronic P123 templated films, (iii) unfunctionalized Brij-56 templated films and (iv) Brij-56 templated mesoporous films where the silica matrix has been functionalized with covalently attached propyl groups inside the porous network. All these mesoporous thin films can be prepared using EISA and exhibit 2D-hexagonal order (for details see Lebold et al.[70]). Again, single molecule fluorescence microscopy provides an excellent tool to extract dynamic information about the diffusion of the Doxorubicin. Interestingly,

in the experiments mostly mobile and immobile populations were found. For example, for P123-templated films, 5% mobile and 95% immobile molecules were observed. The presence of a majority of immobile molecules is surprising. A better understanding of this phenomenon comes from experiments where dependent fluorescence spectra of Doxorubicin were measured (from ensemble to single molecule concentration). With these data sets the immobile molecules can be assigned to be Doxorubicin monomers and the mobile population to be Doxorubicin dimers or multimers (see Supporting Information[70]). During medical applications the delivery system will be loaded with high concentrations of Doxorubicin such that the drug will mainly be present in the form of mobile aggregates. This mobility is essential for the release of the drug.

The evaluated trajectories reveal that Doxorubicin diffuses in a very different manner depending on the choice of the structure directing template. For example, highly structured trajectories were obtained for the mobile population in CTAB templated mesoporous thin films. Fig. 7b displays such a trajectory of a single Doxorubicin molecule, revealing the large linear domains inside the materials.[14] In these films, mobile and immobile molecules were found with a ratio of 1:9. The mean diffusion coefficient $\langle D \rangle$ for the mobile population was determined to be $\langle D_{CTAB} \rangle = 2.0 \times 10^4 \pm 2.3 \times 10^3$ nm^2/s.

Surprisingly, for the unfunctionalized Brij-56 templated samples the evaluation of the recorded movies shows that all molecules were immobile. Fig. 7c displays such an exemplary single molecule "trajectory". It consists of a blue spot, displaying the immobility of the molecule. This strong adsorption of the Doxorubicin can be attributed to the hydroxyl groups in the channel walls.[14,57] The hydroxyl groups interact via hydrogen bonding with the numerous oxygen atoms in the Doxorubicin molecule (see Fig. 7a). Interestingly, in the CTAB templated samples with a narrow pore-to-pore distance of 4.4 nm (compared to 6.1 nm for the unfunctionalized Brij-56 templated film) a mobile population was found. There are several effects that can contribute to the observed mobility in this system. The adsorption sites are shielded by the ionic template CTAB, which electrostatically saturates the channel surface and thus suppresses their capability of forming hydrogen bonds with the drug. Brij-56 is a nonionic template that cannot effectively shield the hydroxyl groups.

This model is supported by the results of another experiment utilizing Brij-56 templated thin films with propyl-functional groups (10 mol%) covering the channel walls This leads to a hydrophobization of the pore inner surface which can be explained by a shielding of the hydroxyl groups. Again a mobile population can be observed (ratio of mobile to immobile molecules for these films ~1:9). Fig. 7d displays an exemplary trajectory of such a mobile molecule. The well-structured trajectory clearly maps the domain structure of the underlying porous network. The mean diffusion coefficient of this mobile population was found to be $\langle D_{propyl-Brij} \rangle = 1.6 \times 10^4 \pm 1.9 \times 10^3$ nm^2/s.

The mobile population in P123-templated films is faster, giving $\langle D_{P123} \rangle = 5.4 \times 10^4 \pm 9.7 \times 10^3$ nm^2 s^{-1} by a factor of ~2.7 compared to the CTAB samples and ~3.4 compared to propyl-functionalized Brij-56 templated films. This can be explained by the increase of the pore-to-pore distance from 4.4 nm (CTAB) to 10 nm (P123).

The described data mark the first time that a clinically relevant drug has been monitored during its motion inside a nanoporous delivery system on a single molecule level. These investigations clearly demonstrate the benefits of a single molecule approach to this study, as the different mobile and immobile populations would have been obscured by the inevitable averaging associated with ensemble methods. Through pore diameter control and pore functionalization the host–guest interactions and the host dynamics can be controlled efficiently.

The next important step towards the use of these materials as drug-delivery systems for Doxorubicin is a measurement of the release kinetics in a live-cell environment. Such data were obtained with P123 templated films since Pluronic is well-known as biocompatible micellar nanocarrier of pharmaceuticals, such as Doxorubicin.[71] Fig. 7e schematically represents the sample setup for the release and live-cell measurements. A coverslip with the Doxorubicin-loaded mesoporous structure can be mounted with a magnet inside the top cover of a μ-Dish directly above HeLa cells in medium. Prior to use, the mesoporous silica film was carefully rinsed with water in order to remove loosely bound Doxorubicin from the film surface, which otherwise could obscure the measurement. Upon removing the magnet on the upper side of the cover, the coverslip is immersed into the cell medium. The medium enters the pores and triggers the Doxorubicin release from the mesoporous system. The increase of Doxorubicin fluorescence can be monitored in the cell medium 50 μm above the bottom of the μ-Dish. Stirring of the entire μ-Dish guarantees a homogeneous distribution of the released Doxorubicin inside the solution. Fig. 7f shows data from an example experiment measuring the increase of Doxorubicin fluorescence intensity (grey curve). Within the first few minutes after adding the drug-loaded coverslip to the cell medium, no Doxorubicin fluorescence could be detected. This delay is the time the cell medium needs to flush the pores and to trigger the drug release. Once the release has started ($t = 0$), the Doxorubicin fluorescence rapidly increases. The data can be fitted to the following exponential equation

$$y = A * \left(1 - \exp-\left(\frac{x}{t_r}\right)\right) \quad (3)$$

where the amplitude A corresponds to the maximum fluorescence intensity and t_r is the characteristic release time. The concurrence between fit and experimental data shows that the release follows a first-order kinetics. By averaging the release times from the experiments, one obtains a mean release-time $\langle t_r \rangle = 3.2$ min $\pm$ 0.8 min. After about 10 min, most of the drug has been released. Thus, a drug incorporated in the delivery system can efficiently be delivered to the surrounding solution. After the release, the thin film is still intact, which can be proven by X-ray diffractometry data (data not shown). Cauda et al. found a similar release kinetics for the antibiotic Vancomycin from mesoporous silica.[72] For an unfunctionalized Brij-56 templated film, where all molecules are immobile (see Fig. 7c), no significant increase in Doxorubicin fluorescence and thus no drug release can be detected in the cell

medium.[70] Therefore the diffusion dynamics in the film directly affects the release kinetics from the film. While these studies present a major breakthrough for the application of mesoporous materials as drug carriers, for therapeutic applications mesoporous structures can also be capped in order to prevent an early release of the drug from the delivery system prior to reaching the target-site.[31,34,73]

Finally, it is important to investigate the effect of the delivered Doxorubicin onto cells. Fig. 7g shows overlay of confocal transmission images (grey) and fluorescence images of the Doxorubicin fluorescence (red). According to their shape, the investigated HeLa cells are alive before being exposed to Doxorubicin (upper left panel). The transmission image shows the adhered cells on the bottom of the μ-Dish. No doxorubicin fluorescence can be detected at this stage of the experiment. After $t = 60$ min, Doxorubicin fluorescence can clearly be located inside the cell nucleus (upper right panel). This can be rationalized as the cytostatic properties of Doxorubicin mainly arise from direct intercalation into DNA as well as inhibition of topoisomerase II by interfering with the topoisomerase II-DNA complex.[74] However, at this incubation time the cells still appear to be alive according to the underlying transmission image. After $t = 24$ h, the cells are highly fluorescing (lower left panel), show a round shape and have detached from the bottom of the μ-Dish, indicating cell death. These effects are caused by the drug itself, as demonstrated by control experiments with a Doxorubicin-free delivery system (lower right panel). This proves that Doxorubicin released from thin films is still cytostatic and the mesoporous films can thus be applied for drug-delivery purposes.

This study highlights the potential of mesoporous silica structures for novel drug-delivery applications in cancer therapy. The application of single molecule techniques offers detailed mechanistic insights into the complicated host–guest interplay. The interaction of the drug with the host matrix can be influenced on a nanometre scale via covalently attached organic functional groups. Such fine-tuning of the host–guest interaction is an essential prerequisite for generating a depot-effect. Furthermore, the drug can be released from the nanochannels in the carrier system and can be taken up by cells. For future applications mesoporous structures could be used either in the form of nanoparticles for drug-delivery applications, for example in cancer therapy, or in the form of film implants or coatings, for example, for the delivery of immunosuppressive drugs to diminish rejection. Hence, a wide range of different drugs is within the scope for this novel class of delivery system.

Outlook to future developments

Mesoporous silica nanomaterials offer a high potential for applications in drug-delivery and nanomedicine. The experiments described in this review provide a solid basis for a thorough understanding of these novel hybrid materials. Yet, in order to assess their applicability in drug-delivery in detail, live-cell imaging studies need to follow that evaluate the effects of the materials onto living cells. Very recent work by Cauda et al.[75] addresses this issue by investigating the effect of the anti-cancer drug colchicine on the depolymerization of the

microtubules. Additionally, Sauer et al.[76] evaluated the role of endosomal escape for disulfide-linkage based drug release from mesoporous silica. Moreover, further studies that critically investigate the toxicity and biodegradability of mesoporous silica need to follow.

We have seen throughout this review that a large amount of information can be gained by investigating mesoporous silica materials with the help of single molecule microscopy. In general, these insights profit fundamentally from a high localization accuracy of the individual fluorophores inside the materials. Yet, a high precision of retrieving the molecular position can not only be achieved by the exact localization of the particle with the help of tracking procedures but also through so-called super-resolution techniques. Recently, several methods to overcome the Abbé resolution limit have been developed, such as stimulated emission depletion (STED)[77] and ground state depletion (GSD)[78] microscopy as well as saturated pattern excitation microscopy (SPEM), also known as saturated structured illumination microscopy (SSIM).[79,80] Additionally, further single molecule based super-resolution techniques such as photoactivatable localization microscopy (PALM)[81,82] and stochastic optical reconstruction micro-scopy (STORM)[83] were developed. These novel techniques offer additional tools to visualize processes on the nanoscale in great detail.

Moreover, the single molecule techniques applied here still bear a high potential for future investigations. As long as the substrates are optically transparent and a suitable fluorophore is chosen, single molecule microscopy is an excellent tool to study these samples. The method is non-invasive, reveals subpopulations and yields real-time information about highly dynamic processes. The ability to record data with a high frame rate even prevails the capabilities of many above mentioned super-resolution techniques. Single molecule microscopy could for example become a powerful method to investigate samples in the emerging field of lab-on-a-chip applications. Studying miniaturized samples that show highly dynamic processes, for example due to molecular separation or catalysis processes inside mesoporous silica channels on a chip, could be highly interesting.

Consequently, single molecule microscopy and novel nano-materials could also in the future form an insightful synergy that reveals many hidden details.

Acknowledgements

References

1 J. S. Beck, J. C. Vartuli, W. J. Roth, M. E. Leonowicz, C. T. Kresge, K. D. Schmitt, C. T. W. Chu, D. H. Olson, E. W. Sheppard, S. B. McCullen, J. B. Higgins and J. L. Schlenker, *J. Am. Chem. Soc.*, 1992, **114**(27), 10834–10843.
2 C. T. Kresge, M. E. Leonowicz, W. J. Roth, C. E. Vartuli and J. S. Beck, *Nature*, 1992, **359**, 710–712.
3 D. Y. Zhao, J. L. Feng, Q. S. Huo, N. Melosh, G. H. Fredrickson, B. F. Chmelka and G. D. Stucky, *Science*, 1998, **279**(5350), 548–552.
4 D. Y. Zhao, Q. S. Huo, J. L. Feng, B. F. Chmelka and G. D. Stucky, *J. Am. Chem. Soc.*, 1998, **120**(24), 6024–6036.
5 F. Schuth and W. Schmidt, *Adv. Mater.*, 2002, **14**(9), 629–638.
6 A. Katiyar, S. Yadav, P. G. Smirniotis and N. G. Pinto, *J. Chromatogr., A*, 2006, **1122**(1–2), 13–20.
7 B. Platschek, N. Petkov and T. Bein, *Angew. Chem., Int. Ed.*, 2006, **45**(7), 1134–1138.
8 V. Cauda, L. Muhlstein, B. Onida and T. Bein, *Microporous Mesoporous Mater.*, 2009, **118**(1–3), 435–442.
9 J. Y. Ying, C. P. Mehnert and M. S. Wong, *Angew. Chem., Int. Ed.*, 1999, **38**(1–2), 56–77.
10 G. Oye, J. Sjoeblom and M. Stoecker, *Adv. Colloid Interface Sci.*, 2001, **89**, 439–466.
11 P. C. A. Alberius, K. L. Frindell, R. C. Hayward, E. J. Kramer, G. D. Stucky and B. F. Chmelka, *Chem. Mater.*, 2002, **14**(8), 3284–3294.
12 S. Besson, T. Gacoin, C. Ricolleau, C. Jacquiod and J. P. Boilot, *J. Mater. Chem.*, 2003, **13**(2), 404–409.
13 F. Cagnol, D. Grosso, G. J. D. A. S. Soler-Illia, E. L. Crepaldi, F. Babonneau, H. Amenitsch and C. Sanchez, *J. Mater. Chem.*, 2003, **13**(1), 61–66.
14 C. Jung, J. Kirstein, B. Platschek, T. Bein, M. Budde, I. Frank, K. Müllen, J. Michaelis and C. Bräuchle, *J. Am. Chem. Soc.*, 2008, **130**(5), 1638–1648.
15 H. Provendier, C. C. Santini, J. M. Basset and L. Carmona, *Eur. J. Inorg. Chem.*, 2003, (11), 2139–2144.
16 P. M. Visintin, R. G. Carbonell, C. K. Schauer and J. M. DeSimone, *Langmuir*, 2005, **21**(11), 4816–4823.
17 T. Maschmeyer, F. Rey, G. Sankar and J. M. Thomas, *Nature*, 1995, **378**(6553), 159–162.
18 T. Yokoi, H. Yoshitake and T. Tatsumi, *J. Mater. Chem.*, 2004, **14**(6), 951–957.
19 K. Yamamoto and T. Tatsumi, *Chem. Lett.*, 2000, (6), 624–625.
20 K. Yamamoto and T. Tatsumi, *Microporous Mesoporous Mater.*, 2001, **44**(SISI), 459–464.
21 S. Angloher and T. Bein, *J. Mater. Chem.*, 2006, **16**(36), 3629–3634.
22 S. Angloher, J. Kecht and T. Bein, *Chem. Mater.*, 2007, **19**(14), 3568–3574.
23 C. E. Fowler, S. L. Burkett and S. Mann, *Chem. Commun.*, 1997, 1769–1770.
24 J. Aguado, J. M. Arsuaga and A. Arencibia, *Ind. Eng. Chem. Res.*, 2005, **44**(10), 3665–3671.
25 S. J. L. Billinge, E. J. McKimmy, M. Shatnawi, H. Kim, V. Petkov, D. Wermeille and T. J. Pinnavaia, *J. Am. Chem. Soc.*, 2005, **127**(23), 8492–8498.
26 D. E. De Vos, M. Dams, B. F. Sels and P. A. Jacobs, *Chem. Rev.*, 2002, **102**(10), 3615–3640.
27 V. Rebbin, R. Schmidt and M. Fröba, *Angew. Chem., Int. Ed.*, 2006, **45**(31), 5210–5214.
28 N. Petkov, N. Stock and T. Bein, *J. Phys. Chem. B*, 2005, **109**(21), 10737–10743.
29 B. Ye, M. L. Trudeau and D. M. Antonelli, *Adv. Mater.*, 2001, **13**(8), 561.
30 D. J. Cott, N. Petkov, M. A. Morris, B. Platschek, T. Bein and J. D. Holmes, *J. Am. Chem. Soc.*, 2006, **128**(12), 3920–3921.
31 C.-Y. Lai, B. G. Trewyn, D. M. Jeftinija, K. Jeftinija, S. Xu, S. Jeftinija and V. S. Y. Lin, *J. Am. Chem. Soc.*, 2003, **125**, 4451–4459.
32 I. Roy, T. Y. Ohulchanskyy, D. J. Bharali, H. E. Pudavar, R. A. Mistretta, N. Kaur and P. N. Prasad, *Proc. Natl. Acad. Sci. U. S. A.*, 2005, **102**(2), 279–284.
33 S. Giri, B. G. Trewyn and V. S. Y. Lin, *Nanomedicine*, 2007, **2**(1), 99–111.

34 S. Giri, B. G. Trewyn, M. P. Stellmaker and V. S. Y. Lin, *Angew. Chem., Int. Ed.*, 2005, **44**(32), 5038–5044.

35 F. Torney, B. G. Trewyn, V. S. Y. Lin and K. Wang, *Nat. Nanotechnol.*, 2007, **2**(5), 295–300.

36 G. Binnig, H. Rohrer, C. Gerber and E. Weibel, *Appl. Phys. Lett.*, 1982, **40**(2), 178–180.

37 G. Binning, H. Rohrer, C. Gerber and E. Weibel, *Phys. Rev. Lett.*, 1982, **49**(1), 57–61.

38 G. Binnig, C. F. Quate and C. Gerber, *Phys. Rev. Lett.*, 1986, **56**(9), 930–933.

39 V. Kukla, J. Kornatowski, D. Demuth, I. Girnus, H. Pfeifer, L. V. C. Rees, S. Schunk, K. K. Unger and J. Kärger, *Science*, 1996, **272**(5262), 702–704.

40 N. E. Benes, H. Jobic and H. Verweij, *Microporous Mesoporous Mater.*, 2001, **43**(2), 147–152.

41 W. E. Moerner and L. Kador, *Phys. Rev. Lett.*, 1989, **62**(21), 2535–2538.

42 W. E. Moerner and M. Orrit, *Science*, 1999, **283**, 1670–1676.

43 M. Orrit and J. Bernard, *Phys. Rev. Lett.*, 1990, **65**(21), 2716–2719.

44 W. E. Moerner and D. P. Fromm, *Rev. Sci. Instrum.*, 2003, **74**(8), 3597–3619.

45 W. E. Moerner, *Proc. Natl. Acad. Sci. U. S. A.*, 2007, **104**(31), 12596–12602.

46 C. Bräuchle, D. C. Lamb and J. Michaelis, *Single Particle Tracking and Single Molecule Energy Transfer*, WILEY-VCH, 2010.

47 F. O. Holtrup, G. R. J. Muller, H. Quante, S. Defeyter, F. C. DeSchryver and K. Mullen, *Chem.–Eur. J.*, 1997, **3**(2), 219–225.

48 C. Jung, B. K. Muller, D. C. Lamb, F. Nolde, K. Mullen and C. Bräuchle, *J. Am. Chem. Soc.*, 2006, **128**(15), 5283–5291.

49 F. Nolde, J. Q. Qu, C. Kohl, N. G. Pschirer, E. Reuther and K. Mullen, *Chem.–Eur. J.*, 2005, **11**(13), 3959–3967.

50 Y. Sakamoto, M. Kaneda, O. Terasaki, D. Y. Zhao, J. M. Kim, G. Stucky, H. J. Shim and R. Ryoo, *Nature*, 2000, **408**(6811), 449–453.

51 A. Zürner, J. Kirstein, M. Doblinger, C. Bräuchle and T. Bein, *Nature*, 2007, **450**(7170), 705–709.

52 C. J. Brinker, Y. F. Lu, A. Sellinger and H. Y. Fan, *Adv. Mater.*, 1999, **11**(7), 579–585.

53 J. Kirstein, B. Platschek, C. Jung, R. Brown, T. Bein and C. Bräuchle, *Nat. Mater.*, 2007, **6**(4), 303–310.

54 R. M. Dickson, D. J. Norris, Y.-L. Tzeng and W. E. Moerner, *Science*, 1996, **274**(5289), 966–968.

55 J. Kirstein, Diffusion of single molecules in nanoporous meso-structured materials, Doctoral Thesis, Ludwig-Maximilians-University Munich, 2007.

56 F. Feil, C. Jung, J. Kirstein, J. Michaelis, L. Chen, F. Nolde, K. Müllen and C. Bräuchle, *Microporous Mesoporous Mater.*, 2009, **125**, 70–78.

57 C. Jung, C. Hellriegel, B. Platschek, D. Wohrle, T. Bein, J. Michaelis and C. Bräuchle, *J. Am. Chem. Soc.*, 2007, **129**(17), 5570–5579.

58 B. J. Scott, G. Wirnsberger and G. D. Stucky, *Chem. Mater.*, 2001, **13**(10), 3140–3150.

59 C. Hellriegel, J. Kirstein, C. Bräuchle, V. Latour, T. Pigot, R. Olivier, S. Lacombe, R. Brown, V. Guieu, C. Payrastre, A. Izquierdo and P. Mocho, *J. Phys. Chem. B*, 2004, **108**(38), 14699–14709.

60 C. Hellriegel, J. Kirstein and C. Bräuchle, *New J. Phys.*, 2005, **7**, 23–36.

61 B. Munoz, A. Ramila, J. Perez-Pariente, I. Diaz and M. Vallet-Regi, *Chem. Mater.*, 2003, **15**(2), 500–503.

62 M. Vallet-Regi, F. Balas and D. Arcos, *Angew. Chem., Int. Ed.*, 2007, **46**(40), 7548–7558.

63 S. Shen, P. S. Chow, F. Chen and R.B. H. Tan, *Chem. Pharm. Bull.*, 2007, **55**(7), 985–991.

64 Q. H. Yang, J. Yang, J. Liu, Y. Li and C. Li, *Chem. Mater.*, 2005, **17**(11), 3019–3024.

65 W. S. Han, Y. Kang, S. J. Lee, H. Lee, Y. Do, Y. A. Lee and J. H. Jung, *J. Phys. Chem. B*, 2005, **109**(44), 20661–20664.

66 T. Lebold, L. A. Mühlstein, J. Blechinger, M. Riederer, H. Amenitsch, R. Köhn, K. Peneva, K. Müllen, J. Michaelis, C. Bräuchle and T. Bein, *Chem.–Eur. J.*, 2009, **15**(7), 1661–1672.

67 D. Wagner, W. V. Kern and P. Kern, *Clinical Investigator*, 1994, **72**(6), 417–423.

68 Y. Collins and S. Lele, *Journal of the National Medical Association*, 2005, **97**, 1414–1416.

69 J. O'Shaughnessy, *Oncologist*, 2003, **8**, 1–2.

70 T. Lebold, C. Jung, J. Michaelis and C. Brauchle, *Nano Lett.*, 2009, **9**(8), 2877–2883.

71 V. P. Torchilin, *Pharm. Res.*, 2007, **24**(1), 1–16.

72 V. Cauda, B. Onida, B. Platschek, L. Muhlstein and T. Bein, *J. Mater. Chem.*, 2008, **18**(48), 5888–5899.

73 A. Schlossbauer, J. Kecht and T. Bein, *Angew. Chem., Int. Ed.*, 2009, **48**, 3092–3095.

74 P. D'Arpa and L. F. Liu, *Biochimica Et Biophysica Acta*, 1989, **989**(2), 163–177.

75 V. Cauda, H. Engelke, A. Sauer, D. Arcizet, C. Brauchle, J. Radler and T. Bein, *Nano Lett.*, 2010, **10**(7), 2484–2492.

76 A. Sauer, A. Schlossbauer, N. Ruthardt, V. Cauda, T. Bein and C. Bräuchle, *Nano Lett.*, 2010, **10**, 3684–3691.

77 S. W. Hell and J. Wichmann, *Opt. Lett.*, 1994, **19**(11), 780–782.

78 S. W. Hell and M. Kroug, *Appl. Phys. B: Lasers Opt.*, 1995, **60**(5), 495–497.

79 R. Heintzmann, T. M. Jovin and C. Cremer, *J. Opt. Soc. Am. A*, 2002, **19**(8), 1599–1609.

80 M. G. L. Gustafsson, *Proc. Natl. Acad. Sci. U. S. A.*, 2005, **102**(37), 13081–13086.

81 E. Betzig, G. H. Patterson, R. Sougrat, O. W. Lindwasser, S. Olenych, J. S. Bonifacino, M. W. Davidson, J. Lippincott-Schwartz and H. F. Hess, *Science*, 2006, **313**(5793), 1642–1645.

82 S. T. Hess, T. P. K. Girirajan and M. D. Mason, *Biophys. J.*, 2006, **91**(11), 4258–4272.

83 M. J. Rust, M. Bates and X. W. Zhuang, *Nat. Methods*, 2006, **3**(10), 793–795.

This journal is © the Owner Societies 2011

Phys. Chem. Chem. Phys., 2011, **13**, 5017–5033 | 5033